ADVANCED MATERIALS
www.advmat.de

Engineering Antimicrobial Metal–Phenolic Network Nanoparticles with High Biocompatibility for Wound Healing

Rongxin Yu, Hongping Chen, Jian He, Zhichao Zhang, Jiajing Zhou, Qinqin Zheng, Zhouping Fu, Chengyin Lu, Zhixing Lin, Frank Caruso,* and Xiangchun Zhang**

Antibiotic-resistant bacteria pose a global health threat by causing persistent and recurrent microbial infections. To address this issue, antimicrobial nanoparticles (NPs) with low drug resistance but potent bactericidal effects have been developed. However, many of the developed NPs display poor biosafety and their synthesis often involves complex procedures and the antimicrobial modes of action are unclear. Herein, a simple strategy is reported for designing antimicrobial metal–phenolic network (am-MPN) NPs through the one-step assembly of a seeding agent (diethyldithiocarbamate), natural polyphenols, and metal ions (e.g., Cu^{2+}) in aqueous solution. The Cu^{2+}-based am-MPN NPs display lower Cu^{2+} antimicrobial concentrations (by 10–1000 times) lower than most reported nanomaterials and negligible toxicity across various models, including, cells, blood, zebrafish, and mice. Multiple antimicrobial modes of the NPs have been identified, including bacterial wall disruption, reactive oxygen species production, and quinoprotein formation, with the latter being a distinct pathway identified for the antimicrobial activity of the polyphenol-based am-MPN NPs. The NPs exhibit excellent performance against multidrug-resistant bacteria (e.g., methicillin-resistant *Staphylococcus aureus* (MRSA)), efficiently inhibit and destroy bacterial biofilms, and promote the healing of MRSA-infected skin wounds. This study provides insights on the antimicrobial properties of metal–phenolic materials and the rational design of antimicrobial metal–organic materials.

1. Introduction

Bacterial infections, which are linked to severe morbidity and mortality, pose a significant global health threat.[1] The overuse and misuse of antibiotics have led to the emergence of multidrug-resistant bacteria (e.g., methicillin-resistant *Staphylococcus aureus* (MRSA)), which could result in an estimated 10 million deaths annually by 2050.[2] Another key factor contributing to antibiotic resistance is the formation of biofilms, wherein an extracellular matrix provides nutrients to bacteria and limits antibiotic penetration.[3] Nanoparticles (NPs) have emerged as promising antimicrobial agents, as they can physically break bacterial membrane barriers and release active components, making it challenging for bacteria to form resistance.[4] For instance, metal NPs (e.g., Cu) can induce bacterial membrane damage by generating reactive oxygen species (ROS). However, the clinical application of metal NPs is restricted by their potentially high toxicity at elevated doses.[5] Furthermore, the requirement for additional external stimuli (e.g., near-

R. Yu, H. Chen, Q. Zheng, Z. Fu, C. Lu, X. Zhang
Tea Research Institute
Chinese Academy of Agricultural Sciences
Hangzhou 310008, China
E-mail: zhangxc@tricaas.com

J. He
College of Basic Medical and Forensic Medicine
Henan University of Science and Technology
Luoyang 471000, China

Z. Zhang
Department of Orthopedics
Shanghai General Hospital
Shanghai Jiao Tong University
Shanghai 200000, China

J. Zhou
College of Biomass Science and Engineering
Sichuan University
Chengdu 610065, China

Z. Lin, F. Caruso
Department of Chemical Engineering
The University of Melbourne
Parkville, Victoria 3010, Australia
E-mail: zhixing.lin@unimelb.edu.au; fcaruso@unimelb.edu.au

The ORCID identification number(s) for the author(s) of this article can be found under https://doi.org/10.1002/adma.202307680

DOI: 10.1002/adma.202307680

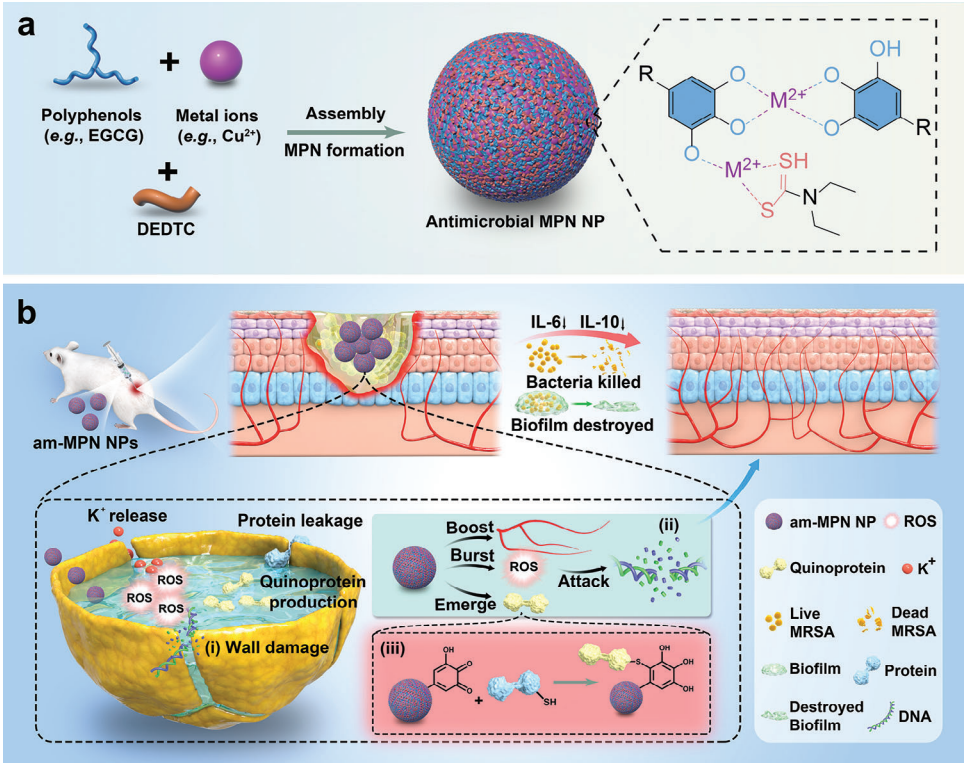

Scheme 1. Schematics of a) synthesis of antimicrobial metal–phenolic network nanoparticles (am-MPN NPs) and b) their antimicrobial modes of action including: i) rupture of bacterial cell walls; ii) generation of reactive oxygen species (ROS), which causes DNA damage; and iii) formation of quinoproteins, which may lead to oxidative stress responses.

infrared radiation for photothermal carbon NPs) and harsh synthesis conditions (e.g., organic solvents), and associated high costs (e.g., antimicrobial peptides) restrict the further development and commercialization of many antimicrobial NPs.[6]

Metal–organic networks are supramolecular materials composed of metal ions and organic ligands and have found a wide range of applications in diverse fields, including chemistry, materials, and biomedical science.[7] Incorporating antimicrobial components (e.g., antimicrobial ligands or noble metal ions) into metal–organic networks has recently attracted increasing attention owing to their potential for long-term antimicrobial behaviors and their reduced cytotoxicity compared to metal NPs.[8] However, the use of synthetic antimicrobial ligands can often require complex synthesis procedures, while using organic ligands solely to act as carriers for metal ions can raise biosafety concerns and compromise antimicrobial efficiency.[9] Therefore, there remains a need to develop a simple strategy for synthesizing antimicrobial metal–organic networks, comprising only highly biocompatible components, with high antimicrobial efficiency against antibiotic-resistant bacteria and related biofilms.

Polyphenols derived from tea are known for their natural ability to protect plants from pathogens and are widely used in the preparation of beverages owing to their antioxidant properties and ability to produce quinone radicals for anticancer therapy.[10] Moreover, polyphenols can coordinate with various metal ions to form coordination networks, termed metal–phenolic networks (MPNs), on various substrates.[11] MPN coatings have been explored for antimicrobial applications on various nonantimicrobial substrates (e.g., polymer particles); however, the introduction of substrates may lower the antimicrobial efficiency of the materials and can cause safety issues.[12] The direct formation of MPN NPs would represent an alternative strategy but is a challenge owing to their rapid chelation process.[13] Therefore, diethyldithiocarbamate (DEDTC) was selected as the coordination modulator and seeding agent to modulate the coordination kinetics of the metal–phenolic complexation processes owing to its strong chelation ability with metal ions, negligible cytotoxicity, and antimicrobial properties.[14] DEDTC is a metabolite of the drug disulfiram that has been approved by the US Food and Drug Administration (FDA) for treating heavy metal poisoning.

Herein, we report a simple strategy for synthesizing antimicrobial MPN (am-MPN) NPs through the one-step assembly of polyphenols (e.g., (−)-epigallocatechin gallate (EGCG)), metal ions (e.g., Cu^{2+}), and DEDTC (**Scheme 1**). Assembly was complete within seconds under aqueous conditions at room temperature. All of the components used are generally recognized as safe by the FDA, and the negligible toxicity of am-MPN NPs is confirmed across various models from cells to blood, zebrafish, nematodes, and mice. The am-MPN NPs exhibit antimicrobial properties against antibiotic-resistant bacteria (e.g., MRSA), even at Cu^{2+} concentrations that are 10–1000 times lower than those for reported Cu-based nanomaterials. Additionally, the am-MPN NPs efficiently inhibit bacterial biofilm formation and destroy biofilms and promote wound healing in MRSA-infected mice. Systematic studies reveal that the antimicrobial modes of action of am-MPNs NPs include the formation of quinoproteins, which

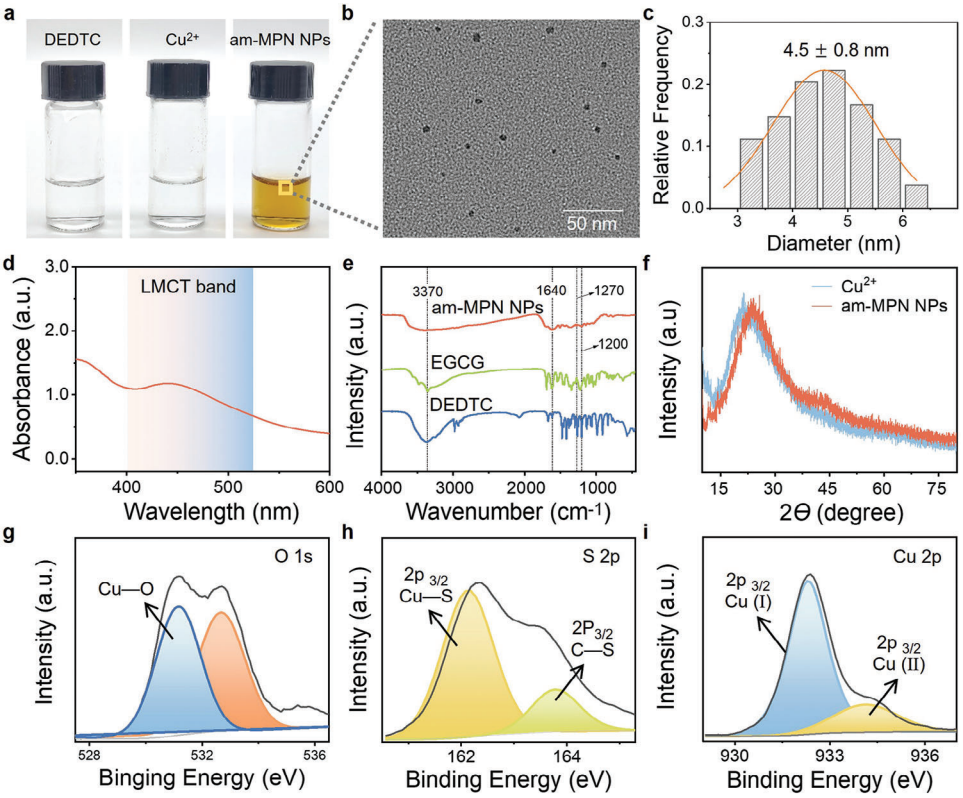

Figure 1. Characterization of antimicrobial metal–phenolic network nanoparticles (am-MPN NPs). a) Photographs of solutions of diethyldithiocarbamate (DEDTC), Cu^{2+}, and am-MPN NPs. b) High-resolution transmission electron microscopy (TEM) image, c) size distribution (from TEM), and d) UV–Visible (UV–Vis) absorption spectrum of am-MPN NPs. e) Fourier transform infrared (FTIR) spectra of (−)-epigallocatechin gallate (EGCG), DEDTC, and am-MPN NPs. f) X-ray diffraction (XRD) patterns of Cu^{2+} and am-MPN NPs. g–i) High-resolution X-ray photoelectron spectroscopy (XPS) spectra of O 1s (g), S 2p (h), and Cu 2p (i) of am-MPN NPs. LMCT, ligand-to-metal charge transfer.

is an antimicrobial pathway specific to the polyphenol-based am-MPN NPs. This work sheds light on the antimicrobial properties of phenolic-based materials and provides a pathway to the rational design of metal–organic materials with promising potential clinical antimicrobial applications.

2. Results and Discussion

2.1. Synthesis and Characterization of am-MPN NPs

The am-MPN NPs were synthesized through the one-step assembly of polyphenols, metal ions, and DEDTC in alkaline solution at room temperature (Scheme 1a and **Figure 1**a and Figure S1, Supporting Information). Note that all three components are inexpensive and commercially available, and have been approved by the FDA for food and medicine formulations, which can expedite potential clinical and commercial translation of am-MPN NPs. The obtained NPs were then characterized using various techniques to determine their morphologies and coordination states (Figure 1). EGCG, a representative tea polyphenol, was chosen as the model polyphenol, and Cu^{2+} was selected as the model metal ion owing to its affordability, widespread use in nutritional supplements, and FDA-approved biomedical applications (e.g., copper-histidine therapy for Menkes disease and cupric sulfate injection for total parenteral nutrition). Moreover, unlike other heavy metal ions (e.g., silver), Cu^{2+} is officially recognized by the US Environmental Protection Agency as an antimicrobial metal owing to its long-term antimicrobial and excellent biosafety properties.[15] The term "am-MPN NPs" refers to the NP system prepared from EGCG, Cu^{2+}, and DEDTC unless otherwise specified. Transmission electron microscopy (TEM) analysis showed that am-MPN NPs were well dispersed and had spherical morphologies with an average diameter of ≈5 nm (Figure 1b,c). The average size of am-MPN NPs, as characterized by DLS, was approximately 30 nm (Figure S2, Supporting Information), which is larger than the size measured by TEM due to the hydration of the NPs. The dominant bis-state metal–phenolic coordination was confirmed by the characteristic ligand-to-metal charge transfer band at ≈430 nm in the UV–Visible (UV–Vis) absorption spectrum (Figure 1d).[16] Fourier transform infrared (FTIR) spectroscopy analysis revealed the presence of C–N peaks at 1270 cm^{-1}, C–O peaks at 1200 cm^{-1}, and HO–C peak at 3370 cm^{-1}, confirming the incorporation of DEDTC and EGCG in the am-MPN NPs (Figure 1e).[17] The am-MPN NPs displayed the same X-ray diffraction (XRD) pattern as free Cu^{2+}, suggesting that Cu^{2+} within the NPs was not oxidized and the amorphous nature of the NPs (Figure 1f).[18] The composition and coordination states of am-MPN NPs were further verified using X-ray photoelectron spectroscopy (XPS). The survey spectrum confirmed the presence of Cu, O, and S originating from the three different

components (i.e., Cu^{2+}, EGCG, and DEDTC; Figure S3, Supporting Information), and the peaks at 531.13, 162.23, and 932.38 eV were assigned to coordination bonds between Cu–PhOH (signal from O 1s), Cu–S (signal from S 2p), and Cu–S (signal from Cu 2p), respectively (Figure 1g–i).[19] In addition, the am-MPN NPs were highly negatively charged (i.e., –48 ± 2 mV) owing to deprotonation of the phenolic compounds (Figure S4, Supporting Information). This results in their high stability during long-term storage (e.g., 3 months), as demonstrated by negligible changes in absorption and Cu^{2+} leakage, as determined by UV–Vis spectroscopy and inductively coupled plasma mass spectrometry (ICP-MS, Figures S5–S7, Supporting Information).

2.2. In Vitro Antimicrobial Activity

The antimicrobial activity of am-MPN NPs was first assessed in vitro by evaluating bacterial growth in solution and by a plate counting method without requiring any external stimuli (e.g., near-infrared radiation). The growth of Gram-positive bacteria (i.e., MRSA, *Staphylococcus epidermidis* (*S. epidermidis*), and *Staphylococcus aureus* (*S. aureus*)) and Gram-negative bacteria (i.e., *Escherichia coli* (*E. coli*), *Pseudomonas aeruginosa* (*P. aeruginosa*)) was monitored by plotting the optical density at 600 nm (OD_{600}) over time at varying concentrations of am-MPN NPs (**Figure 2**a–c and Figure S8, Supporting Information). The concentration of the am-MPN NPs was calculated and normalized by the Cu^{2+} concentration using ICP-MS to facilitate comparison with other Cu^{2+}-based materials. The survival rates of the Gram-positive and Gram-negative bacteria under different treatment conditions were then assessed, and the am-MPN NPs exhibited excellent antimicrobial performance against Gram-positive bacteria, including different antibiotic-resistant bacterial strains (Figure 2d and Figure S9, Supporting Information). No apparent antimicrobial activity against MRSA was observed when evaluating the individual components used for NP synthesis even at high concentrations (e.g., 10×10^{-6} M DEDTC or 5×10^{-6} M Cu^{2+}), indicating the synergistic antimicrobial effects arising from the different components of am-MPN NPs (Figure 2d and Figure S10, Supporting Information). The am-MPN NPs exhibited negligible antimicrobial effects against the Gram-negative bacteria (Figure 2c and Figures S8 and S11, Supporting Information). The treated bacteria were subsequently collected and purified, and the loading amounts of am-MPN NPs inside the bacteria were visualized and quantified (Figure S12, Supporting Information). A larger quantity of NPs entered the Gram-positive bacteria (e.g., MRSA) than the Gram-negative bacteria (e.g., *E. coli*) though these bacteria possess similar surface charges (Figure S12c, Supporting Information). Notably, the selective antimicrobial behavior was also observed with the am-MPN NPs prepared from other polyphenols (i.e., EGCG, epicatechin (EC), epicatechin gallate (ECG), and epigallocatechin (EGC)) and metal ions (i.e., Ag^{+}, Mg^{2+}, Au^{3+}, and Pt^{4+}) (Figure S13, Supporting Information). The selective antibacterial behavior of am-MPN NPs could potentially reduce the development of resistant bacteria and be useful for biomedical applications in the intestine areas where probiotic bacteria need to be preserved.[20]

The antimicrobial behavior of am-MPN NPs was further characterized in solid agar plates by quantifying viable bacteria using colony-forming units (CFUs). Specifically, equal amounts of the bacteria studied were incubated with am-MPN NPs at different concentrations and then evenly spread on agar plates. The turbidity and CFUs of the Gram-positive bacteria decreased significantly with increasing concentrations of am-MPN NPs (Figure 2e). For instance, am-MPN NPs completely eliminate MRSA with a low concentration of 2.5×10^{-6} M, which is significantly lower than those of most reported Cu^{2+}-based nanomaterials in achieving comparable, or lower, inhibition rates (Figure 2e and Tables S1 and S2, Supporting Information). In contrast, no significant changes were observed for the treated Gram-negative bacteria at either of the NP concentrations examined, further confirming the selective antimicrobial behavior of am-MPN NPs (Figure 2e and Table S2, Supporting Information). This selective antimicrobial behavior was further demonstrated by incubating a mixture of *S. aureus* and *E. coli* to 5×10^{-6} M am-MPN NPs for 8 h. As observed in Figure S14 (Supporting Information), all *S. aureus* colonies died and the number of CFUs in *E. coli* only changed minimally. The selective antimicrobial behavior of am-MPN NPs against Gram-positive (over Gram-negative) bacteria is likely due to either the lack of a physical outer membrane barrier in Gram-positive bacteria or the presence of specific membrane antigens in Gram-positive bacteria that bind to am-MPN NPs.[21]

2.3. Inhibition of Bacterial Biofilm Formation and Destruction of Bacterial Biofilms

Biofilms are complex communities of bacteria that form a self-supporting matrix composed of diverse nutrients, such as polysaccharides, proteins, and extracellular DNA.[22] This matrix provides a protective shield that helps bacteria survive in harsh environments, including exposure to antibiotics, and is a primary driver of drug resistance and recurrent infections. Therefore, we evaluated the antimicrobial efficacy of am-MPN NPs against a model biofilm consisting of multidrug-resistant bacteria (i.e., MRSA; **Figure 3**a). We first investigated the ability of am-MPN NPs to inhibit MRSA biofilm formation. The biofilm was labeled using crystal violet staining and quantified by measuring the intensity of absorbance at 595 nm using UV–Vis spectroscopy. As the concentration of am-MPN NPs increased, the staining of the bacteria solution became lighter, indicating a reduction in biofilm formation. For example, relative to the biofilm area formed in the absence of NP treatment, the biofilm area was reduced to 22% when MRSA was treated with 2.5×10^{-6} M am-MPN NPs (Figure 3b–e). This inhibitory effect was further confirmed by inverted microscopy imaging (Figures S15 and S16, Supporting Information). The bacteria were stained by live/dead assays and visualized using confocal laser scanning microscopy (CLSM). The CLSM images showed that 5×10^{-6} M am-MPN NPs efficiently inhibited biofilm formation and eradicated more than 92% of multidrug-resistant bacteria (Figure 3e and Figure S17, Supporting Information), partially due to the efficient release of Cu^{2+} from the NPs within the bacterial biofilm (Figure S18, Supporting Information). In contrast, limited inhibition was displayed by the individual components (i.e., EGCG, DEDTC, and Cu^{2+}) for MRSA biofilm formation, suggesting the synergistic antibacterial ability of these components within am-MPN NPs (Figure S19, Supporting Information).

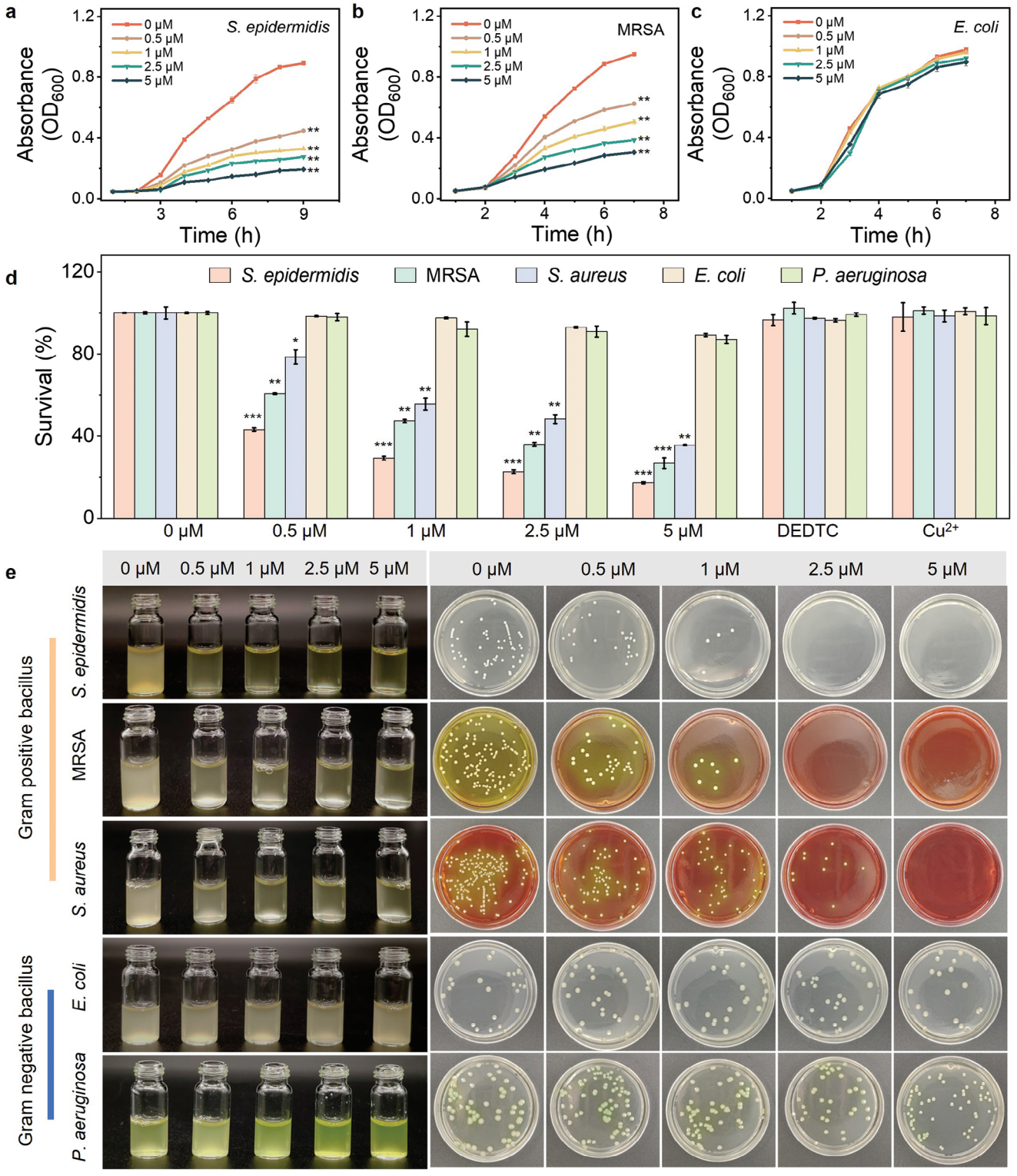

Figure 2. In vitro antimicrobial activity of antimicrobial metal–phenolic network nanoparticles (am-MPN NPs). a–c) Growth curves of *Staphylococcus epidermidis (S. epidermidis)*, methicillin-resistant *Staphylococcus aureus* (MRSA), and *Escherichia coli* (*E. coli*) upon incubation with am-MPN NPs at different concentrations (0–5 × 10^{-6} M). d) Survival rates of bacteria after incubating with am-MPN NPs (at varied concentrations of 0, 0.5 × 10^{-6}, 1 × 10^{-6}, 2.5 × 10^{-6}, and 5 × 10^{-6} M), diethyldithiocarbamate (DEDTC) (10 × 10^{-6} M), or Cu^{2+} (5 × 10^{-6} M) for 8 h. e) Photographs showing the antimicrobial activity of am-MPN NPs in solution and on agar plates. Data are presented as the mean ± standard deviation (s.d.), $^{*}p < 0.05$, $^{**}p < 0.01$, $^{***}p < 0.001$.

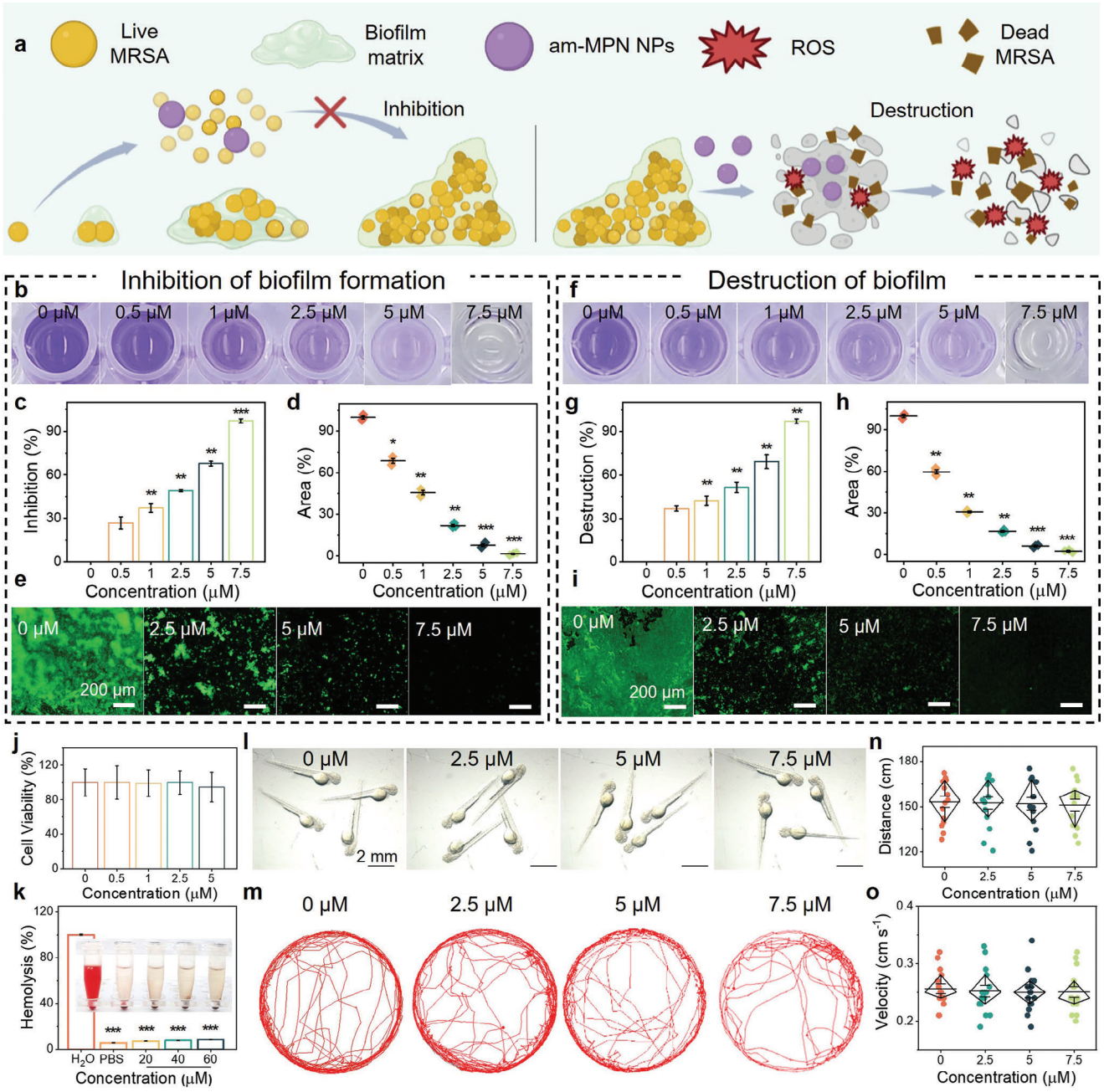

Figure 3. Biofilm formation inhibition and biofilm destruction, and biosafety of antimicrobial metal–phenolic network nanoparticles (am-MPN NPs). a) Schematic diagram of am-MPN NPs inhibiting biofilm formation and destroying preformed biofilms. b) Photographs showing the inhibition of methicillin-resistant *Staphylococcus aureus* (MRSA) biofilm formation by am-MPN NPs at varying concentrations (0–7.5 × 10^{-6} M) after crystal violet staining. c) Quantitative analysis of MRSA biofilm formation inhibition observed in (b). d) Quantitative analysis of MRSA biofilm areas observed in (e). e) Live staining assay of the inhibition of MRSA biofilm formation upon incubation with am-MPN NPs at different concentrations. f) Photographs showing the destruction of preformed MRSA biofilm by am-MPN NPs at varying concentrations (0–7.5 × 10^{-6} M) after crystal violet staining. g) Quantitative analysis of MRSA biofilm destruction observed in (f). h) Quantitative analysis of MRSA biofilm areas observed in (i). i) Live staining assay of the destruction of preformed MRSA biofilm upon incubation with am-MPN NPs at different concentrations. j,k) Cytotoxicity of am-MPN NPs at different concentrations to human umbilical vein endothelial cells (HUVECs) (j) and mouse red blood cells (k). Note that no statistically significant difference was observed in the cytotoxicity data of am-MPN NPs at different concentrations to HUVECs. l–o) Cytotoxicity of am-MPN NPs at different concentrations to zebrafish, as quantified by changes in their morphology (l), trajectory (m), distance traveled (n), and swimming speed (o). Data are presented as the mean ± s.d., $^{*}p < 0.05$, $^{***}p < 0.001$.

Moreover, we demonstrate that am-MPN NPs can destroy preformed bacterial biofilms in a concentration-dependent manner. As the concentration of am-MPN NPs increased, the originally intact MRSA biofilm structure became thinner and was eventually destroyed (Figure 3f–i and Figures S20 and S21, Supporting Information), which is potentially promising for the clinical treatment of patients with bacterial infections. Similar antimicrobial effects of am-MPN NPs were observed for the other Gram-positive bacterial biofilms examined (*S. epidermidis* and *S. aureus*) (Figures S22–S24, Supporting Information).

2.4. Biocompatibility and Biosafety of am-MPN NPs

The biocompatibility and biosafety of am-MPN NPs were investigated before exploring their potential for in vivo applications. am-MPN NPs at varying concentrations were incubated with human umbilical vein endothelial cells (HUVECs) and mouse NIH/3T3 cells. Negligible cytotoxicity was observed for both cell lines, even at high particle concentrations (Figure 3j and Figures S25 and S26, Supporting Information). For instance, after incubation with 5×10^{-6} M am-MPN NPs for 24 h, ≈95% of HUVECs survived, whereas MRSA was completely eradicated under the same conditions on solid agar plates (Figure 2e and Figure 3j). A hemolysis assay was subsequently performed to evaluate the effect of am-MPN NPs on the rupture and lysis of mouse red blood cells. The results showed that even at high concentrations (e.g., 60×10^{-6} M), am-MPN NPs did not cause any apparent hemolysis, indicating their high blood biocompatibility (Figure 3k). Furthermore, the cytotoxicity of am-MPN NPs was evaluated via the zebrafish embryo acute toxicity test. As observed from the data in Figure 3l, no significant changes were observed in the zebrafish morphology after incubating with am-MPN NPs for 36 h. The locomotor behavior of zebrafish was also assessed and quantified (Figure 3m). The swimming distance and velocity of the zebrafish after incubating with 7.5×10^{-6} M am-MPN NPs were 151.0 ± 15.1 cm and 0.25 ± 0.03 cm s^{-1}, respectively, which are comparable to those obtained without treatment (i.e., 153.3 ± 14.5 cm and 0.26 ± 0.03 cm s^{-1}), indicating the negligible cytotoxicity of the NPs (Figure 3m–o). The negligible cytotoxicity of am-MPN NPs for long-term biosafety was further demonstrated in two types of nematode strains (i.e., N2 and TJ375) throughout their entire lifespan of approximately 2 weeks (Figure S27, Supporting Information). Overall, these findings demonstrate that am-MPN NPs exhibit high in vitro and in vivo biocompatibility, supporting their further development for clinical applications.

2.5. In Vivo Antimicrobial Activity and Wound Healing

The wound healing potential of am-MPN NPs was first investigated by conducting HUVEC-based migration assays. HUVECs were mechanically scratched to stimulate a wound and then incubated with am-MPN NPs at different concentrations for 24 h. The migration percentages increased from 2% to 88% with increasing concentrations of am-MPN NPs from 0.2×10^{-6} to 1.0×10^{-6} M (Figure S28, Supporting Information), indicating that am-MPN NPs could efficiently promote the migration of HUVECs at low concentrations. Subsequently, the performance of am-MPN NPs was evaluated in a mouse model with MRSA-infected skin wounds (**Figure 4**a). Groups of 10 mice were administered with am-MPN NPs at different doses or control agents on Days 1 and 3 and monitored until Day 7. Phosphate-buffered saline (PBS) and vancomycin (Van) were selected as the negative and positive controls for MRSA-infected skin wound healing. Wounds without bacterial infection (labeled as Un-inf) healed naturally with a wound area reduced to 17.5 ± 10.8 mm^2, whereas PBS-treated wounds remained with a wound area of 44.3 ± 11.2 mm^2 after 7 days, demonstrating the successful preparation of the MRSA-infected model (Figure 4b,c and Figure S29 and Table S3, Supporting Information). am-MPN NPs at two different doses (20×10^{-6} M, am-MPN NPs-1; 40×10^{-6} M, am-MPN NPs-2) were administered to the mice. Both doses efficiently promoted wound healing by reducing the infected skin wound areas to 34.8 ± 9.2 and 17. 5 ± 8.8 mm^2 by Day 7 (Figure 4b,c and Table S3, Supporting Information). The performance of am-MPN NPs-2 was comparable to or better than that of Van (wound area measured on Day 7 was 20.7 ± 5.0 mm^2). Van, a glycopeptide, is considered a last resort antibiotic and can cause severe side effects.[23] Furthermore, there were no significant changes in the body weight, blood routine, or biochemistry of the mice after incubating with am-MPN NPs (Figure 4d and Figures S30 and S31, Supporting Information).

Histopathological analysis was performed to assess the epithelial gap and capillary density of the MRSA-infected skin wound tissues. The results revealed that treatment with am-MPN NPs shortened the epithelial gap and enhanced capillary density (Figure 4e–g) relative to treatment with the controls. Notably, treatment with am-MPN NPs promoted the formation of blood vessels, as consistent with the ability of the NPs to promote HUVEC migration (Figure 4 g and Figure S28, Supporting Information). Immunohistochemistry (IHC) was employed to evaluate the expression levels of inflammatory cytokines interleukin-6 (IL-6) and interleukin-10 (IL-10), which are essential indicators of bacterial infection in animals. The infected wound tissue of the PBS group showed high amounts of IL-6 and IL-10, which could aggravate the inflammatory response in mice (Figure 4e and Figure S32, Supporting Information). In contrast, treatment with am-MPN NPs or Van regulated the secretion of inflammatory factors (e.g., IL-6 and IL-10) and proliferative markers (e.g., Ki67, platelet endothelial cell adhesion molecule-1 (CD31), and α-smooth muscle actin (α-SMA)) to normal levels, thus effectively reducing the inflammatory response (Figure 4e and Figure S32, Supporting Information). The amount of MRSA in the infected wound tissues was further quantified using the agar plate method. The wound tissues were collected after treatment for 7 days and cultured in Luria–Bertani broth medium. The MRSA CFU count in mice treated with am-MPN NPs or Van was significantly lower than in mice treated with PBS, further confirming the in vivo antimicrobial potential of am-MPN NPs (Figure 4 h). Moreover, no significant pathological abnormalities were observed in the heart, liver, spleen, lung, or kidney of the mice after treatment (Figure S33, Supporting Information). Collectively, these findings demonstrate that am-MPN NPs possess high biocompatibility, low bactericidal concentration, inflammatory cytokine regulating ability, and the ability to promote MRSA-infected wound healing in vivo.

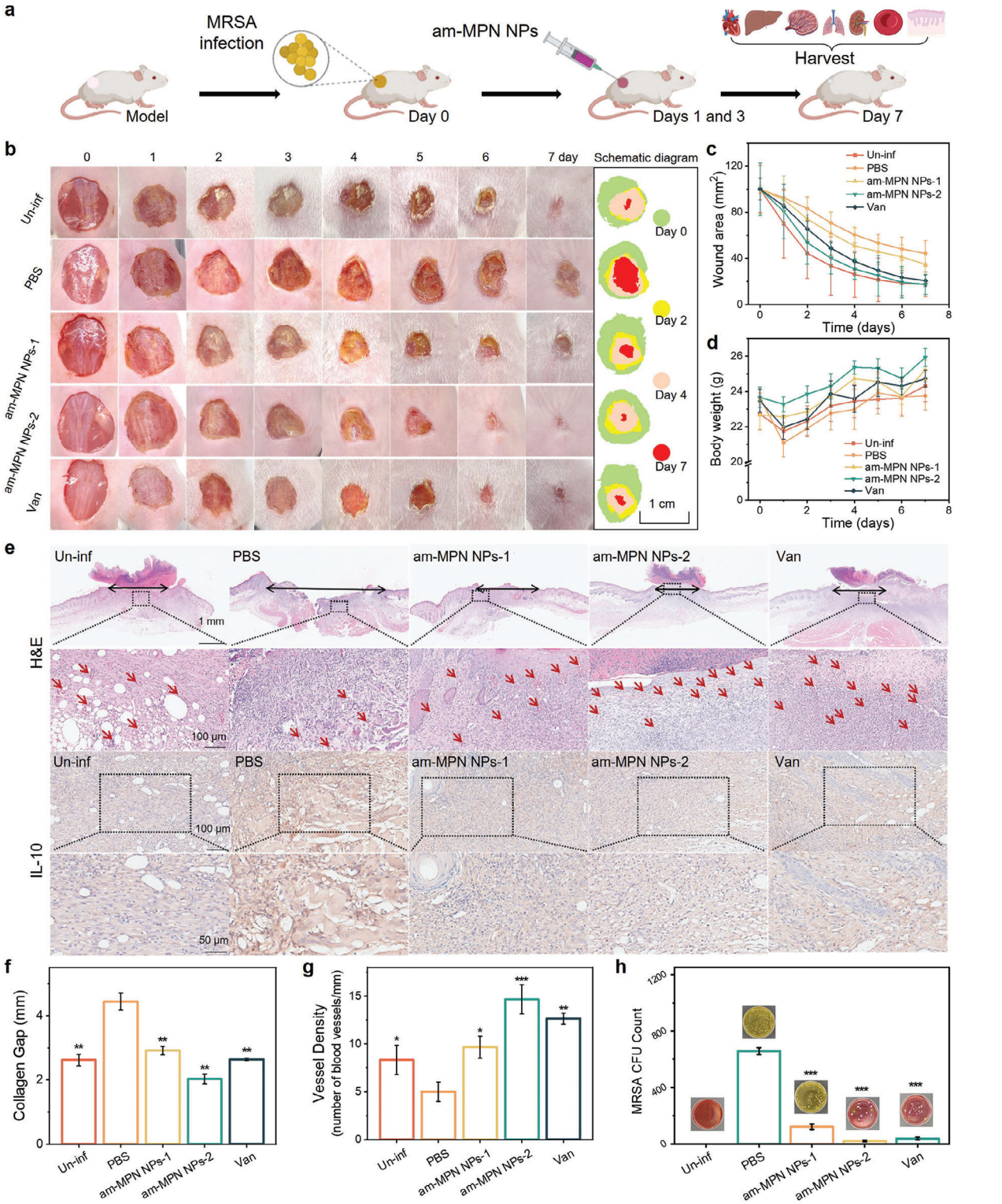

Figure 4. Antimicrobial metal–phenolic network nanoparticles (am-MPN NPs) accelerate methicillin-resistant *Staphylococcus aureus* (MRSA) infected wound healing in vivo. a) Schematic of the treatment of MRSA-infected mice with am-MPN NPs. b) Photographs of changes in wound in MRSA-infected mice after treatment with Van (control) or am-MPN NPs (at varying doses) for 7 days. The Un-inf group represents uninfected skin wounds. c,d) Changes in infected wound area (c) and body weight (d) of mice subjected to different treatments. e) Evaluation of infected skin wound tissue by hematoxylin and eosin (H&E) staining and IHC of interleukin-10 (IL-10) after treatments. Red arrows indicate the formation of blood vessels. f) Analysis of collagen gap in different treatment groups. g) Vessel density of wound healing tissue sites after different treatments. h) Evaluation of bacterial colonies inside infected skin after different treatments. Error bars represent s.d. ($n = 10$). $^{*}p < 0.05$, $^{**}p < 0.01$, $^{***}p < 0.001$.

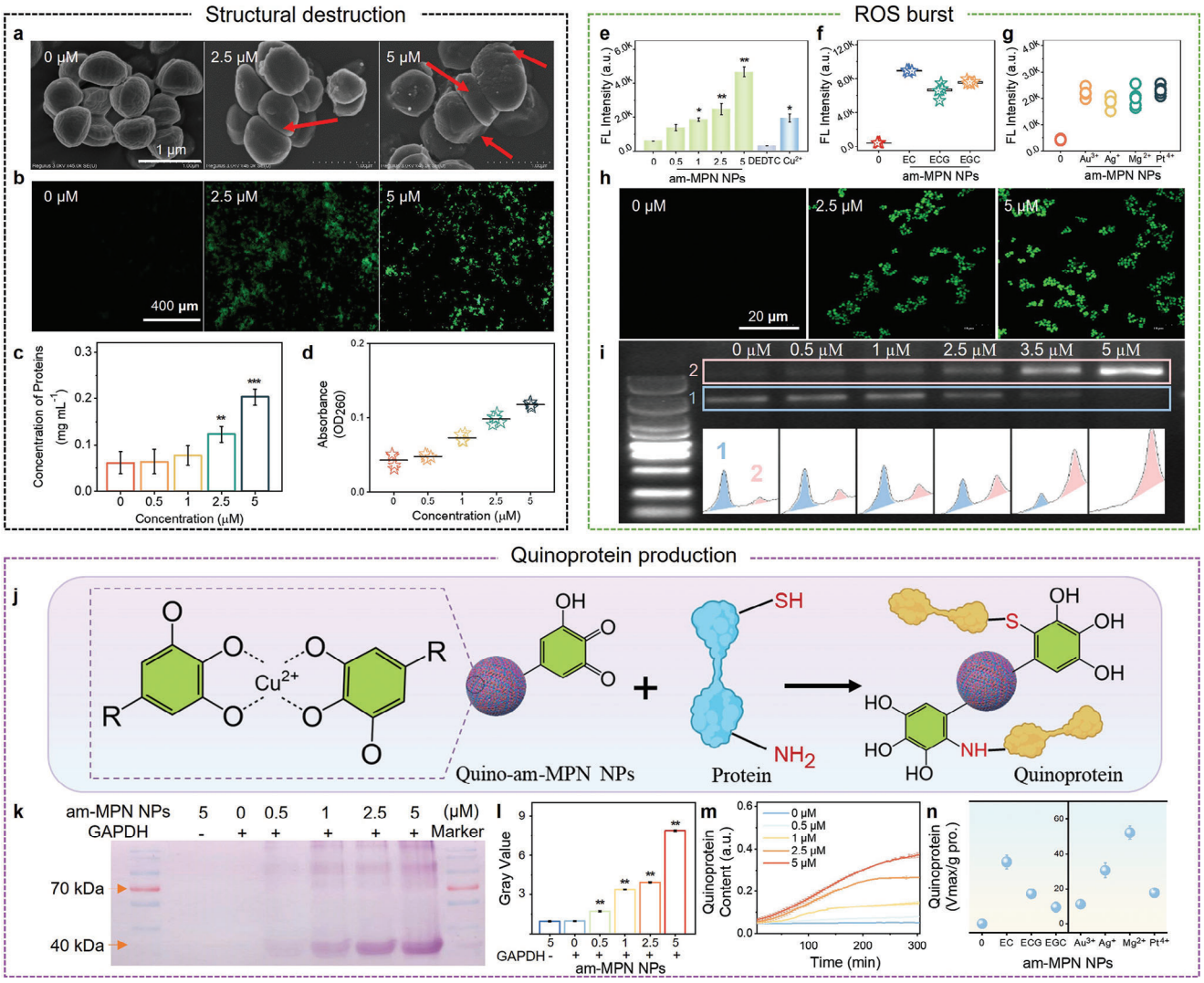

Figure 5. Elucidation of the antibacterial modes of action of antimicrobial metal–phenolic network nanoparticles (am-MPN NPs). a) Scanning electron microscopy (SEM) images of methicillin-resistant *Staphylococcus aureus* (MRSA) treated with or without am-MPN NPs. Red arrows indicate the destruction of the wall and membrane structures of MRSA. b) Confocal laser scanning microscopy (CLSM) images of MRSA biofilms following treatment with or without am-MPN NPs. The MRSA biofilm was labeled with $DiBAC_4(3)$ fluorescence (FL) probe to monitor cell membrane rupture. c,d) Leakage of protein (c) and nucleic acids (d) from MRSA after treatment with am-MPN NPs at different concentrations. e–g) Reactive oxygen species (ROS) burst triggered by different am-MPN NPs. h) CLSM imaging of endogenous ROS formed in MRSA upon treatment with am-MPN NPs. i) Gel electrophoresis analysis indicating DNA fragmentation caused by am-MPN NPs. j) Schematic of the formation of quinoproteins in cells owing to the presence of polyphenols in am-MPN NPs. k) Qualitative assessment of quinoprotein formation after treatment with am-MPN NPs at different concentrations in vitro. l) Quantification of quinoprotein amounts from analysis in (k). m) Quantitative assessment of quinoprotein formation in MRSA during treatment with am-MPN NPs. n) Quantitative assessment of quinoprotein formation in MRSA after treatment with am-MPN NPs fabricated from different phenolic ligands and metal ions. Vmax and pro represent the maximum rate of quinone protein production and protein content in bacteria, respectively. EC, epicatechin; ECG, epicatechin gallate; EGC, epigallocatechin. Data are presented as the mean ± s.d. ($n = 6$). $^{*}p < 0.05$, $^{**}p < 0.01$, $^{***}p < 0.001$.

2.6. Antibacterial Modes of Action of am-MPN NPs

The antimicrobial modes of action of the am-MPN NPs against Gram-positive bacteria were investigated. As observed from the scanning electron microscopy (SEM) images in **Figure 5**a, the wall and membrane structures of MRSA were destroyed upon treatment with am-MPN NPs, whereas PBS-treated MRSA retained intact wall and membrane structures. The voltage-sensitive dye, bis-(1,3-dibutylbarbituric acid) trimethine oxonol ($DiBAC_4(3)$), was used to monitor the hyperpolarization and disassembly of cell membranes.[24] The fluorescence (FL) signal observed upon treating MRSA with am-MPN NPs indicates damage to the bacterial wall membrane (Figure 5b). The ruptured cell walls led to the leakage of a variety of intracellular components, such as proteins, K^+, and DNA, which were characterized using different techniques (e.g., bicinchoninic acid protein assay; Figure 5c,d and Figures S34–S38, Supporting Information). Furthermore, similar DNA leakages were observed in the other treated Gram-positive bacteria (i.e., *S. epidermidis* and *S. aureus*) but not the treated Gram-negative bacteria (i.e., *E. coli*

and *P. aeruginosa*) (Figures S39 and S40, Supporting Information), consistent with the results discussed earlier. Collectively, these results suggest that am-MPN NPs can effectively disrupt the MRSA membrane, triggering the release of DNA, proteins, and K^+ from MRSA into the extracellular medium (Figure 5a–d). Furthermore, as deduced from Figures S35 and S38 (Supporting Information), am-MPN NPs significantly outperformed the individual components.

In addition to disrupting cell walls, am-MPN NPs produced ROS that attack key macromolecules within the bacterial cell to cause bacteria death.[25] The amount of ROS produced in the presence of am-MPN NPs was concentration-dependent and significantly higher than that generated in the presence of the individual components (Figure 5e and Figure S41, Supporting Information). We also observed the production of ROS in MRSA and related bactericidal behaviors in am-MPN NPs fabricated from different metal ions (i.e., Au^{3+}, Ag^+, Mg^{2+}, and Pt^{4+}) and phenolic ligands (i.e., EC, ECG, and EGC) (Figure 5f,g and Figures S1 and S42–S45, Supporting Information). The high levels of ROS within the treated MRSA were further visualized by CLSM (Figure 5h). Moreover, the high level of ROS produced by am-MPN NPs could denature supercoiled DNA into nicked DNA in a concentration-dependent manner, as shown by gel electrophoresis (Figure 5i and Figure S46, Supporting Information).[26]

The phenolic groups EGCG in am-MPN NPs are prone to undergo oxidation to form electron-deficient semiquinones in the presence of Cu^{2+}, which can bind to sulfhydryl residues on proteins and result in the formation of quinoproteins (quinone–protein conjugates) (Figure 5j).[27] Although these quinoproteins have been observed to induce a cascade of cell apoptosis.[28] their existence and potential applications in antimicrobial fields remain unexplored. To detect and quantify the amount of quinoproteins, a redox–cycling staining assay was employed, wherein quinoproteins convert colorless nitroblue tetrazolium into insoluble purple formazan in the presence of glycine.[29] Glyceraldehyde-3-phosphate dehydrogenase (GAPDH), a widely distributed housekeeping enzyme, was chosen as a model protein to investigate the in vitro production of quinoproteins.[30] am-MPN NPs at different concentrations were incubated with a GAPDH solution, followed by staining using the redox–cycling assay and analysis by agarose gel electrophoresis. The appearance of purple bands on the sodium dodecyl-sulfate polyacrylamide gel indicated the concentration-dependent formation of quinoproteins (Figure 5k,l). In addition, the in vivo production of quinoprotein was observed by incubating MRSA with am-MPN NPs at different concentrations for 4 h and quantified by measuring the optical density at 530 nm using a microplate reader (Figure 5m and Figures S47 and S48, Supporting Information). In contrast, treatment with DEDTC (10×10^{-6} м) or Cu^{2+} (5×10^{-6} м) alone did not result in quinoprotein production, indicating the key role of phenolic ligands in forming quinoproteins (Figure S48, Supporting Information). The overabundance of quinoproteins in MRSA disrupts the redox homeostasis and potentially deactivates the functional enzymes containing reactive cysteines (which necessitates further in-depth and systematic investigation), leading to catastrophic events in bacterial cells and eventually bacterial death.[31] We also demonstrate that diverse am-MPN NPs fabricated from various phenolic ligands and metal ions are all capable of producing quinoproteins (Figure 5n and Figure S49, Supporting Information).

3. Conclusion

We developed a simple strategy for synthesizing am-MPN NPs by the one-step assembly of polyphenols, metal ions, and DEDTC. The components used in the synthesis are all FDA-approved, and the negligible cytotoxicity of the resulting NPs was demonstrated across various models, including human cells, blood, zebrafish, and mice. The am-MPN NPs exhibited antimicrobial activity against multidrug-resistant bacteria (e.g., MRSA), both in vitro and in vivo, with one of the lowest Cu^{2+} bactericidal concentrations (i.e., 2.5 μm) reported in the literature. The modes of action of antimicrobial activity of the am-MPN NPs were also investigated and identified, including bacteria cell membrane destruction, ROS production, and bacteria DNA deactivation. Notably, a quinoprotein production-based antimicrobial pathway, which is specific to the polyphenol-based am-MPN NPs, was unveiled. Considering the excellent antimicrobial efficacy, low toxicity, and facile synthesis of the am-MPN NPs, these NPs are potentially promising for clinical applications, particularly in treating antibiotic-resistant bacterial infections. This work also provides insights into the antimicrobial properties of polyphenol-based materials and paves the way for the rational design of metal–organic NPs for biomedical applications.

Supporting Information

Supporting Information is available from the Wiley Online Library or from the author.

Acknowledgements

R.Y. and H.C. contributed equally to this work. This work was supported by the Key Research and Development Program of Zhejiang (2023C02040), the National Natural Science Foundation of China (32372757 and 32001013), the innovative Program of Chinese Academy of Agricultural Sciences (Y2022QC24, CAAS-ASTIP-2021-TRI), and the Australian Research Council (ARC) through the Discovery Project (DP200100713) scheme. F.C. acknowledges the award of a National Health and Medical Research Council Leadership Fellowship (GNT2016732).

Open access publishing facilitated by The University of Melbourne, as part of the Wiley - The University of Melbourne agreement via the Council of Australian University Librarians.

Conflict of Interest

The authors declare no conflict of interest.

Data Availability Statement

The data that support the findings of this study are available from the corresponding author upon reasonable request.

Keywords

biofilms, metal–organic materials, polyphenols, quinoprotein, selective antimicrobial

Received: July 31, 2023
Revised: November 2, 2023
Published online:

[1] a) C. Nathan, *Nat. Rev. Microbiol.* **2020**, *18*, 259; b) L. S. J. Roope, R. D. Smith, K. B. Pouwels, J. Buchanan, L. Abel, P. Eibich, C. C. Butler, P. S. Tan, A. S. Walker, J. V. Robotham, S. Wordsworth, *Science* **2019**, *364*, eaau4679; c) S. H. E. Kaufmann, A. Dorhoi, R. S. Hotchkiss, R. Bartenschlager, *Nat. Rev. Drug Discovery* **2018**, *17*, 35; d) A. Mullard, *Nat. Rev. Drug Discovery* **2016**, *15*, 447.

[2] a) C. Willyard, *Nature* **2017**, *543*, 15; b) P. Tan, C. Wu, Q. Tang, T. Wang, C. Zhou, Y. Ding, H. Fu, S. Xu, Y. Feng, Y. Zhang, Q. Dai, X. Ma, *Adv. Mater.* **2023**, *35*, 2210766; c) Y. Cheng, Y. Zhang, Z. Zhao, G. Li, J. Li, A. Li, Y. Xue, B. Zhu, Z. Wu, X. Zhang, *Adv. Mater.* **2022**, *34*, 2206646; d) C. G. Starr, J. Ghimire, S. Guha, J. P. Hoffmann, Y. Wang, L. Sun, B. N. Landreneau, Z. D. Kolansky, I. M. Kilanowski-Doroh, M. C. Sammarco, L. A. Morici, W. C. Wimley, *Proc. Natl. Acad. Sci. U. S. A.* **2020**, *117*, 8437; e) J. O'Neill, https://amr-review.org/sites/default/files/160518_Final%20paper_with%20cover.pdf (accessed: July **2023**).

[3] a) K. Sauer, P. Stoodley, D. M. Goeres, L. Hall-Stoodley, M. Burmølle, P. S. Stewart, T. Bjarnsholt, *Nat. Rev. Microbiol.* **2022**, *20*, 608; b) H. Koo, R. N. Allan, R. P. Howlin, P. Stoodley, L. Hall-Stoodley, *Nat. Rev. Microbiol.* **2017**, *15*, 740; c) R. E. W. Hancock, M. A. Alford, E. F. Haney, *Nat. Rev. Microbiol.* **2021**, *19*, 786; d) C. J. Nobile, E. P. Fox, J. E. Nett, T. R. Sorrells, Q. M. Mitrovich, A. D. Hernday, B. B. Tuch, D. R. Andes, A. D. Johnson, *Cell* **2012**, *148*, 126.

[4] a) Y. Liu, L. Shi, L. Su, H. C. Van Der Mei, P. C. Jutte, Y. Ren, H. J. Busscher, *Chem. Soc. Rev.* **2019**, *48*, 428; b) Y. Wang, Y. Yang, Y. Shi, H. Song, C. Yu, *Adv. Mater.* **2020**, *32*, 1904106; c) B. Peng, X. Zhang, D. G. A. L. Aarts, R. P. A. Dullens, *Nat. Nanotechnol.* **2018**, *13*, 478.

[5] a) T. Cai, G. Fang, X. Tian, J.-J. Yin, C. Chen, C. Ge, *ACS Nano* **2019**, *13*, 12694; b) P. Gao, Y. Chen, W. Pan, N. Li, Z. Liu, B. Tang, *Angew. Chem., Int. Ed.* **2021**, *60*, 16763.

[6] a) E. Zhang, X. Zhao, J. Hu, R. Wang, S. Fu, G. Qin, *Bioact. Mater.* **2021**, *6*, 2569; b) Q. Xin, H. Shah, A. Nawaz, W. Xie, M. Z. Akram, A. Batool, L. Tian, S. U. Jan, R. Boddula, B. Guo, Q. Liu, J. R. Gong, *Adv. Mater.* **2019**, *31*, 1804838; c) K. Lu, T. Aung, N. Guo, R. Weichselbaum, W. Lin, *Adv. Mater.* **2018**, *30*, 1707634; d) A. Jacobs, G. Renaudin, C. Forestier, J.-M. Nedelec, S. Descamps, *Acta Biomater.* **2020**, *117*, 21.

[7] a) H. Geng, Q.-Z. Zhong, J. Li, Z. Lin, J. Cui, F. Caruso, J. Hao, *Chem. Rev.* **2022**, *122*, 11432; b) Y. Han, Z. Lin, J. Zhou, G. Yun, R. Guo, J. J. Richardson, F. Caruso, *Angew. Chem., Int. Ed.* **2020**, *59*, 15618; c) J. Zhou, Z. Lin, M. Penna, S. Pan, Y. Ju, S. Li, Y. Han, J. Chen, G. Lin, J. J. Richardson, I. Yarovsky, F. Caruso, *Nat. Commun.* **2020**, *11*, 4804.

[8] a) Y. Li, Y. Miao, L. Yang, Y. Zhao, K. Wu, Z. Lu, Z. Hu, J. Guo, *Adv. Sci.* **2022**, *9*, 2202684; b) J. Fei, J. Zhao, C. Du, A. Wang, H. Zhang, L. Dai, J. Li, *ACS Nano* **2014**, *8*, 8529; c) J. Guo, W. Sun, J. P. Kim, X. Lu, Q. Li, M. Lin, O. Mrowczynski, E. B. Rizk, J. Cheng, G. Qian, J. Yang, *Acta Biomater.* **2018**, *72*, 35; d) B. Hu, Y. Shen, J. Adamcik, P. Fischer, M. Schneider, M. J. Loessner, R. Mezzenga, *ACS Nano* **2018**, *12*, 3385; e) N. Ninan, A. Forget, V. P. Shastri, N. H. Voelcker, A. Blencowe, *ACS Appl. Mater. Interfaces* **2016**, *8*, 28511.

[9] a) T. Simon-Yarza, A. Mielcarek, P. Couvreur, C. Serre, *Adv. Mater.* **2018**, *30*, 1707365; b) K. Chattopadhyay, M. Mandal, D. K. Maiti, *ACS Appl. Bio Mater.* **2021**, *4*, 8159; c) S. Wang, C. M. Mcguirk, A. D'aquino, J. A. Mason, C. A. Mirkin, *Adv. Mater.* **2018**, *30*, 1800202.

[10] a) S. Quideau, D. Deffieux, C. Douat-Casassus, L. Pouységu, *Angew. Chem., Int. Ed.* **2011**, *50*, 586; b) J. Zhou, Z. Lin, Y. Ju, M. A. Rahim, J. J. Richardson, F. Caruso, *Acc. Chem. Res.* **2020**, *53*,1269; c) Y. Shen, H. Lin, M. Yang, X. Gong, B. Guan, Y. Han, S. Wang, Y. Wang, *Adv. Mater.* **2023**, *35*, 2210936.

[11] a) H. Ejima, J. J. Richardson, K. Liang, J. P. Best, M. P. Van Koeverden, G. K. Such, J. Cui, F. Caruso, *Science* **2013**, *341*, 154; b) J. Guo, Y. Ping, H. Ejima, K. Alt, M. Meissner, J. J. Richardson, Y. Yan, K. Peter, D. Von Elverfeldt, C. E. Hagemeyer, F. Caruso, *Angew. Chem., Int. Ed.* **2014**, *53*, 5546; c) J. Guo, B. L. Tardy, A. J. Christofferson, Y. Dai, J. J. Richardson, W. Zhu, M. Hu, Y. Ju, J. Cui, R. R. Dagastine, I. Yarovsky, F. Caruso, *Nat. Nanotechnol.* **2016**, *11*, 1105; d) Z. Lin, J. Zhou, Y. Qu, S. Pan, Y. Han, R. P. M. Lafleur, J. Chen, C. Cortez-Jugo, J. J. Richardson, F. Caruso, *Angew. Chem., Int. Ed.* **2021**, *60*, 24968.

[12] a) Y. Q. Qin, J. Wang, C. Qiu, Y. Hu, X. Xu, Z. Jin, *ACS Sustainable Chem. Eng.* **2019**, *77*, 17379; b) P. Liu, X. Shi, S. Zhong, Y. Peng, Y. Qi, J. Ding, W. Zhou, *Biomater. Sci.* **2021**, *9*, 2825.

[13] a) Z. Lin, J. J. Richardson, J. Zhou, F. Caruso, *Nat. Rev. Chem.* **2023**, *7*, 273; b) J. Chen, S. Pan, J. Zhou, Z. Lin, Y. Qu, A. Glab, Y. Han, J. J. Richardson, F. Caruso, *Adv. Mater.* **2022**, *34*, 2108624; c) W. Xu, Z. Lin, S. Pan, J. Chen, T. Wang, C. Cortez-Jugo, F. Caruso, *Angew. Chem., Int. Ed.* **2023**, *62*, 202312925.

[14] a) P. K. Gessner, T. Gessner, *Disulfiram and Its Metabolite, Diethyldithiocarbamate*, Springer, Dordrecht, Netherlands **1992**. b) Z. Skrott, M. Mistrik, K. K. Andersen, S. Friis, D. Majera, J. Gursky, T. Ozdian, J. Bartkova, Z. Turi, P. Moudry, M. Kraus, M. Michalova, J. Vaclavkova, P. Dzubak, I. Vrobel, P. Pouckova, J. Sedlacek, A. Miklovicova, A. Kutt, J. Li, J. Mattova, C. Driessen, Q. P. Dou, J. Olsen, M. Hajduch, B. Cvek, R. J. Deshaies, J. Bartek, *Nature* **2017**, *552*, 194.

[15] a) S. Mahmoodi, A. Elmi, S. Hallaj Nezhadi, *J. Mol. Pharm. Org. Process Res.* **2018**, *6*, 1000140; b) J. Konieczny, Z. Rdzawski, *Arch. Mater. Sci.* **2012**, *56*, 53.

[16] W. Xu, S. Pan, B. B. Noble, J. Chen, Z. Lin, Y. Han, J. Zhou, J. J. Richardson, I. Yarovsky, F. Caruso, *Angew. Chem., Int. Ed.* **2022**, *61*, 202208037.

[17] K. S. Siddiqi, S. A. A. Nami, Y. C. Lutfullah, *Inorg. Nano-Met. Chem.* **2005**, *35*, 445.

[18] X. Wang, Q. Shi, Z. Zha, D. Zhu, L. Zheng, L. Shi, X. Wei, L. Lian, K. Wu, L. Cheng, *Bioact. Mater.* **2021**, *6*, 4389.

[19] a) K. L. Chavez, D. W. Hess, *J. Electrochem. Soc.* **2001**, *148*, G640; b) R. Scheer, H. J. Lewerenz, *J. Vac. Sci. Technol., A* **1994**, *12*, 56; c) L. M. Engelhardt, P. C. Healy, R. M. Shephard, B. W. Skelton, A. H. White, *Inorg. Chem.* **1988**, *27*, 2371.

[20] a) J. M. V. Makabenta, A. Nabawy, C.-H. Li, S. Schmidt-Malan, R. Patel, V. M. Rotello, *Nat. Rev. Microbiol.* **2021**, *19*, 23; b) A. M. Grumezescu, *Drug Targeting and Stimuli Sensitive Drug Delivery Systems*, William Andrew, Norwich, NY, USA **2018**; c) R. Y. Pelgrift, A. J. Friedman, *Adv. Drug Delivery Rev.* **2013**, *65*, 1803.

[21] a) J. C. Henderson, S. M. Zimmerman, A. A. Crofts, J. M. Boll, L. G. Kuhns, C. M. Herrera, M. S. Trent, *Annu. Rev. Microbiol.* **2016**, *70*, 255; b) A. Konovalova, D. E. Kahne, T. J. Silhavy, *Annu. Rev. Microbiol.* **2017**, *71*, 539; c) S. Yan, S. Chen, X. Gou, J. Yang, J. An, X. Jin, Y.-W. Yang, L. Chen, H. Gao, *Adv. Funct. Mater.* **2019**, *29*, 1904683.

[22] a) L. Hall-Stoodley, J. W. Costerton, P. Stoodley, *Nat. Rev. Microbiol.* **2004**, *2*, 95; b) H.-C. Flemming, J. Wingender, *Nat. Rev. Microbiol.* **2010**, *8*, 623.

[23] a) I. G. Boneca, G. Chiosis, *Expert Opin. Ther. Targets* **2003**, *7*, 311; b) N. A. Turner, B. K. Sharma-Kuinkel, S. A. Maskarinec, E. M. Eichenberger, P. P. Shah, M. Carugati, T. L. Holland, V. G. Fowler Jr., *Nat. Rev. Microbiol.* **2019**, *17*, 203; c) D. L. Paterson, P. N. A. Harris, *Lancet Infect. Dis.* **2016**, *16*, 132.

[24] a) Y. Weng, H. Chen, X. Chen, H. Yang, C.-H. Chen, H. Tan, *Nat. Commun.* **2022**, *13*, 4712; b) X. Wang, L. Tian, J. Fu, S. Liao, S. Yang, X. Jia, G. Gong, *Food Control* **2022**, *131*, 108435.

[25] a) F. Gao, T. Shao, Y. Yu, Y. Xiong, L. Yang, *Nat. Commun.* **2021**, *12*, 745; b) F. Vatansever, W. C. M. A. De Melo, P. Avci, D. Vecchio, M. Sadasivam, A. Gupta, R. Chandran, M. Karimi, N. A. Parizotto, R. Yin, G. P. Tegos, M. R. Hamblin, *FEMS Microbiol. Rev.* **2013**, *37*, 955;

c) D. J. Dwyer, J. J. Collins, G. C. Walker, *Annu. Rev. Pharmacol. Toxicol.* **2015**, *55*, 313; d) J. J. Foti, B. Devadoss, J. A. Winkler, J. J. Collins, G. C. Walker, *Science* **2012**, *336*, 315.

[26] a) M. Liu, L. Huang, X. Xu, X. Wei, X. Yang, X. Li, B. Wang, Y. Xu, L. Li, Z. Yang, *ACS Nano* **2022**, *16*, 9479; b) Y. Li, W. Zhang, J. Niu, Y. Chen, *ACS Nano* **2012**, *6*, 5164; c) J. Du, J. M. Gebicki, *Int. J. Biochem. Cell Biol.* **2004**, *36*, 2334; d) S. He, J. Huang, Q. Zhang, W. Zhao, Z. Xu, W. Zhang, *Adv. Funct. Mater.* **2021**, *31*, 2105198.

[27] a) R. L. Nicholson, R. Hammerschmidt, *Annu. Rev. Phytopathol.* **1992**, *30*, 369; b) C. S. Yang, T. Chen, C.-T. Ho, *J. Agric. Food Chem.* **2022**, *70*, 7887.

[28] a) L. Zhang, Y. He, X. Wu, G. Zhao, K. Zhang, C. S. Yang, R. J. Reiter, J. Zhang, *Cells* **2019**, *8*, 745; b) K. Zhang, R. Dong, K. Sun, X. Wang, J. Wang, C. S. Yang, J. Zhang, *Free Radicals Biol. Med.* **2017**, *113*, 143.

[29] L. Yang, L. Jia, X. Li, K. Zhang, X. Wang, Y. He, M. Hao, M. P. Rayman, J. Zhang, *Food Chem.* **2022**, *386*, 132812.

[30] a) T. Ishii, T. Mori, T. Tanaka, D. Mizuno, R. Yamaji, S. Kumazawa, T. Nakayama, M. Akagawa, *Free Radicals Biol. Med.* **2008**, *45*, 1384; b) Z. Zhang, M. Hao, X. Zhang, Y. He, X. Chen, E. W. Taylor, J. Zhang, *Trends Food Sci. Technol.* **2023**, *132*, 40.

[31] N. Shu, Q. Cheng, E. S. J. Arnér, M. J. Davies, *Redox Biol.* **2020**, *28*, 101335.